lajss.org
Latin American Journal of Solids and Structures
www.lajss.org

Reconciling the strain-stretching curve with the stress-strain diagram of a Hooke-like isotropic hyperelastic material using the Biot's hyperbolic sine strain tensor

Danel Boy Vasconcellos[a*], Marcelo Greco[a]

[a] Universidade Federal de Minas Gerais, Programa de Pós-Graduação em Engenharia de Estruturas, Belo Horizonte, MG, Brasil.
Email: danielvasconcellos@ufmg.br, mgreco@dees.ufmg

* Corresponding author

Abstract

Materials subjected to moderate/large strains that exhibit similar tension and compression trends on the stress-strain diagram have several applications. Inspired by this aspect of this diagram, we have found appropriate to incorporate a same tension and compression trend on the strain-stretching curve of these materials. Because previous literature lacks strain measures with this property, this study intends to obtain this using a strain tensor belonging to a recently introduced strain measure family, the Generalized Hyperbolic Sine (GHS) strain tensor, which has significantly improved the behavior of the Seth-Hill family toward measures with better physical consistency. One uses the positional formulation of the finite element method to obtain expressions for any Lagrangian work conjugate stress-strain pair. Thereafter, this pair is employed in Hooke's law to obtain the constitutive equation. The derivatives of the strain tensors with respect to the deformation gradient are written directly in the global directions and do not explicitly depend on the derivatives of the right stretch tensor with respect to the deformation gradient. Finally, the aforementioned model is used to perform 3D simulations of compressible bodies, including a comparison with a typical result of a polymer foam obtained from literature. The numerical results demonstrate excellent agreement with the analytical results, showing that a reconciliation of the stress-strain diagram of a Hooke-like material with its strain-stretching curve is numerically feasible.

Keywords

strain measures, generalized hyperbolic sine, hooke-like material model, positional formulation of the finite element method

Graphical Abstract

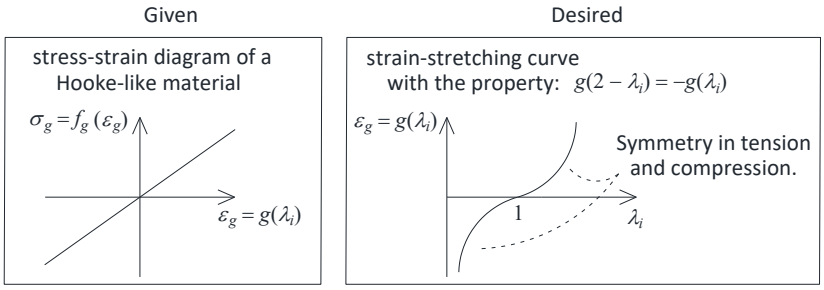

(σ_g , ε_g) is a work-conjugate stress-strain pair.

List of main symbols *Uppercase (lowercase) bold letters are second-order tensors (vectors).*

λ_i: stretching; $\mathbf{U}$: right stretch tensor; $[U_{ij}]$, $[\mathbf{U}]$: matrix representation of $\mathbf{U}$; $\boldsymbol{\alpha}_i$: eigenvectors of $\mathbf{U}$; φ: material parameter of Itskov strain; κ: material parameter of the exponential strain of Darijani and Naghdabadi (2013); ε: arbitrary maximum stretching limit; β: material parameter of GHS strain; γ: real constant of the Seth-Hill family; ${}^{\text{hs}}\mathbf{E}^{(\beta)}$: GHS strain tensor; ${}^{\text{B}}\mathbf{E}^{(\beta)}$: GHS-Biot strain tensor; $\mathbf{F}$: deformation gradient; $\mathbf{T}$, $\mathbf{E}$: arbitrary Lagrangian work conjugate stress-strain pair; $\mathbf{T}$: Cauchy stress tensor; $\mathbf{S}$: second Piola-Kirchhoff stress tensor; μ, λ: Lamé parameters; E: Young's modulus; ν: Poisson ratio; ε_V: volumetric strain.

List of abbreviations

GHS: generalized hyperbolic sine; NGHL: natural generalization of Hooke's law; PFFEM: positional formulation of the finite element method; AP: axial problem; EBP: equi-biaxial problem; SS-PStrain: simple shear in plane strain; SS-PStress: simple shear in plane stress

1 INTRODUCTION

In the computational mechanics of isotropic hyperelastic bodies, different strain energy density functions (depending on the principal stretches and/or the principal invariants of the right Cauchy-Green tensor) have been proposed to better fit the experimental data, as can be seen in Dal et al. (2021) and references therein. Another approach to model these materials is the use of different strain measures, as demonstrated in Doyle & Ericksen (1956), Seth (1964), Curnier & Rakotomanana (1991), Itskov (2004), Curnier & Zysset (2006), Srinivasa (2012), Salamatova et al. (2018), Darijani et al. (2010), Darijani & Naghdabadi (2013), Boujelben & Ibrahimbegovic (2017), Korobeynikov (2019), Greco & Peixoto (2022), and Peixoto et al. (2024).

Once the strain measure is chosen, it can be used by means of the Natural Generalization of Hooke's Law (NGHL) proposed by Hill (1978). This constitutive equation is written by replacing the stress-strain pair of Hooke's law with any work conjugate stress-strain pair. The direct use of Hooke's law for large strains, considering the Cauchy stress tensor as a function of the displacement gradient tensor, does not lead to an objective constitutive equation, as demonstrated by Fosdick & Serrin (1979). Thus, the study of new strain measures is of remarkable importance and is useful for the modeling of polymers and biological tissues (see, e.g., Saucedo-Mora et al. (2021), Korobeynikov (2023), and Kang et al. (2024)).

In addition to guaranteeing the existence of the strain energy density, as noted by Volokh (2004), NGHL has the advantage of using constants (Young's Modulus E and Poisson ratio ν) that are easily known for most materials. One of the most well-known stress-strain pairs used together with NGHL is the second Piola-Kirchhoff stress tensor and the Green strain tensor (St. Venant-Kirchhoff model), although it has limitations in large strain regimes, as pointed out by Sautter et al. (2022). Recent applications of NGHL include those of Korobeynikov (2019), Korobeynikov et al. (2022), Greco & Peixoto (2022), Korobeynikov (2023), Korobeynikov & Larichkin (2023), and Peixoto et al. (2024).

In this context, this study applies a strain measure belonging to the Generalized Hyperbolic Sine (GHS) strain family, recently introduced in Peixoto et al. (2024), to simulate 3D models. One of the main objectives is to include the same behavior in tension and compression on the strain-stretching curve of a given material with an odd function on the stress-strain diagram. This study considers a linear function in this diagram because it uses NGHL. Finally, the numerical results were obtained using the aforementioned constitutive equation for the axial problem, equibiaxial problem, simple shear under plane strain, and simple shear under plane stress.

Following Hill (1978), the general class of Lagrangian strain tensors is defined as (henceforth, the Einstein summation is adopted, and all indices range from 1 to 3 unless stated otherwise)

$$\mathbf{G}(\mathbf{U}) = g(\lambda_i)(\boldsymbol{\alpha}_i \otimes \boldsymbol{\alpha}_i), \tag{1}$$

where λ_i and $\boldsymbol{\alpha}_i$ are the eigenvalues (principal stretches) and the normalized eigenvectors of the right stretch tensor $\mathbf{U}$, respectively, and g: $\mathbb{R}_+^* \to \mathbb{R}$ is a scale function. Based on postulates on the form of the strain energy density, g should satisfy some properties (Hill, 1978; Darijani et al., 2010), namely,

$$g(1)=0, \quad g'(1)=1, \quad g'(\lambda_i)>0, \quad \lim_{\lambda_i \to 0} g(\lambda_i) = -\infty \quad \text{and} \quad \lim_{\lambda_i \to \infty} g(\lambda_i) = \infty . \tag{2}$$

In addition, a specific type of symmetry for g was presented by Truesdell & Toupin (1960), Fitzgerald (1980), and Curnier & Rakotomanana (1991),

$$g(\lambda_i^{-1}) = -g(\lambda_i). \tag{3}$$

Two strain families that follow Equations (2) and (3) are

$$g(\lambda_i)=\frac{1}{2\varphi}(\lambda_i^{\varphi}-\lambda_i^{-\varphi}) \quad \text{and} \qquad (\varphi\in\mathbb{R}_+^*) \tag{4}$$

$$g(\lambda_i)=\frac{1}{2\kappa}\left[e^{\kappa(\lambda_i-1)}-e^{\kappa(\lambda_i^{-1}-1)}\right], \qquad (\kappa\in\mathbb{R}_+^*) \tag{5}$$

where Equation (4) is the strain family introduced by Itskov (2004) and also mentioned by Darijani & Naghdabadi (2010); Equation (5) is the one-parameter exponential strain family introduced by Darijani & Naghdabadi (2013). The Hencky strain ($\ln\lambda_i$) is obtained using Equation (4) as $\varphi\to 0$. Figure 1 shows the plots of the Equations (4) and (5) for certain values of φ and κ.

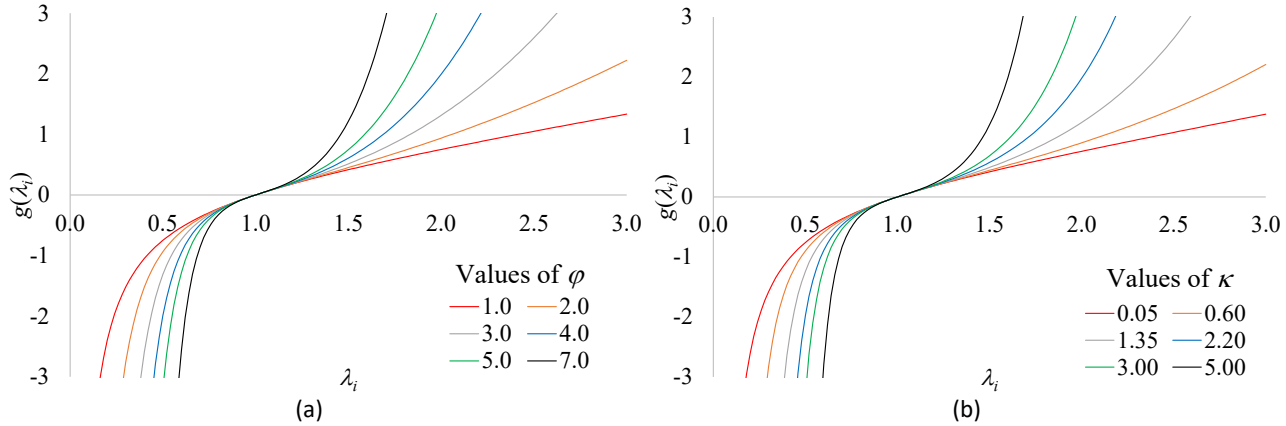

Figure 1 – (a) Strain family of Itskov (2004) for some values of φ. (b) One-parameter exponential family of Darijani & Naghdabadi (2013) for some values of κ.

Notably, a similar behavior in tension and compression tends to be observed only when φ and κ increase. Now, with Equation (2) in mind, an issue arises if one wants to model a material that has the same behavior in tension and compression for any value of the parameter, that is, one wants an odd function shifted by one unit to the right on the strain-stretching curve. As the original definition of the odd function is $-g(\lambda_i)=g(-\lambda_i)$, the desired property is

$$g(2-\lambda_i)=-g(\lambda_i). \tag{6}$$

The Biot strain tensor $\mathbf{U}-\mathbf{I}$, where $\mathbf{I}$ is the second-order unit tensor, obeys Equation (6) but is not concerned with Equation $(2)_4$ at all. The point here is to establish a measure that follows Equation (6) and has some physical consistency in the sense of the Equation (2). One points out that property of the Equation (3) does not lead to the desired symmetry of behavior in tension and compression, and Equation (3) is replaced by Equation (6).

Evidently, Equations (4) and (5) do not follow Equation (6). In fact, Equations (2) and (6) are not completely consistent; that is, given a function that obeys Equation (6), at the best chance, Equation $(2)_4$ or $(2)_5$ will fall. For example, one may introduce the tangent strain

$$g(\lambda_i)=\frac{2}{\pi}\tan\left[\frac{\pi}{2}(\lambda_i-1)\right], \qquad \lambda_i\in\,]0,\,2[\tag{7}$$

which follows Equation (6). However, among the requirements stated in Equation (2), only Equation $(2)_5$ does not hold. A related strain measure to Equation (7), namely, the hyperbolic tangent strain, was introduced by Peixoto & Greco (2022). Figure 2a shows a graph of Equation (7).

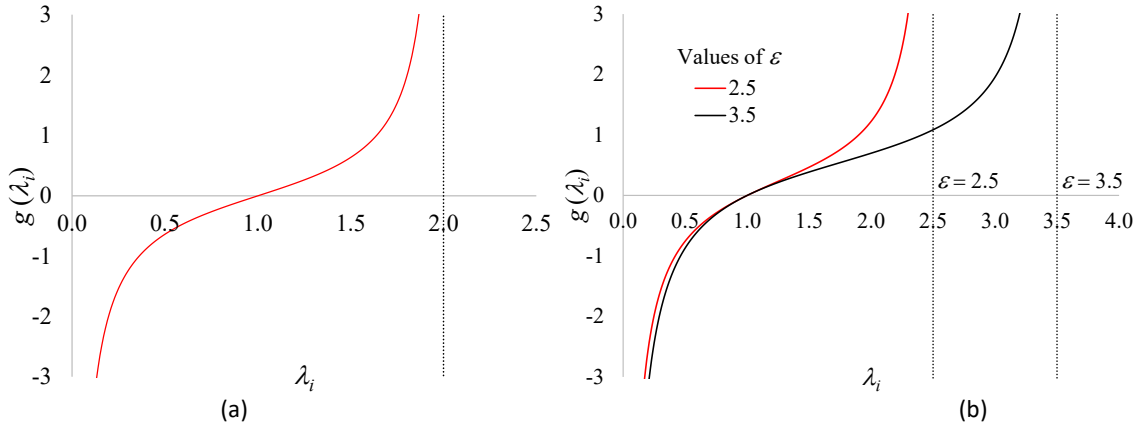

Figure 2 – (a) Tangent strain (Equation (7)). (b) Two curves of tangent strain family.

Apart from Equation (6) for a while, Equation (7) can be improved to include an arbitrary maximum stretching limit $\varepsilon > 1$,

$$g(\lambda_i) = \frac{\varepsilon}{\pi}\cos^2\left[\pi\left(\frac{1}{\varepsilon}-\frac{1}{2}\right)\right]\left\{\tan\left[\pi\left(\frac{\lambda_i}{\varepsilon}-\frac{1}{2}\right)\right]-\tan\left[\pi\left(\frac{1}{\varepsilon}-\frac{1}{2}\right)\right]\right\}. \qquad \lambda_i \in \,]0,\, \varepsilon[\qquad \varepsilon > 1.0 \tag{8}$$

Figure 2b shows the two curves of Equation (8). As shown in Figure 2, it might be interesting to model a material exhibiting a rapid increase in stress at high stretch values (strain-stiffening effect) using a strain measure that incorporates this phenomenon. Experimental data have demonstrated this effect (Treloar, 1975; Arruda & Boyce, 1993), which has played a central role in several studies (Horgan & Saccomandi (2006); Yuan et al. (2015); Cao et al. (2016); Liang et al. (2020); Lateefi et al. (2022)). It should be noted that property of the Equation $(2)_5$ is not a general axiom because rubber-like material behavior may not meet it.

Turning back to pursuing a candidate strain for Equation (6), bearing Equation (2) in mind, let us describe the GHS strain family introduced by Peixoto et al. (2024),

$${}^{\mathrm{hs}}\mathbf{E}^{(\beta)} = \beta^{-1}\sinh\left(\beta\,\mathbf{E}^{(\gamma)}\right), \qquad (\beta \in \mathbb{R}^{*}_{+}) \tag{9}$$

where $\mathbf{E}^{(\gamma)}$ is, *a priori*, any given strain measure. Considering $\mathbf{E}^{(\gamma)}$ as the Seth-Hill Lagrangian family (Seth, 1964; Hill, 1968),

$$\mathbf{E}^{(\gamma)} = \begin{cases} \gamma^{-1}\left(\mathbf{U}^{\gamma}-\mathbf{I}\right) & \gamma \neq 0 \\ \ln \mathbf{U} & \gamma = 0 \end{cases}, \qquad (\gamma \in \mathbb{R}) \tag{10}$$

we can set $\gamma = 1.0$ to obtain the GHS-Biot subfamily ${}^{\mathrm{B}}\mathbf{E}^{(\beta)}$,

$${}^{\mathrm{B}}\mathbf{E}^{(\beta)} = \beta^{-1}\sinh\left(\beta\left(\mathbf{U}-\mathbf{I}\right)\right) = \frac{1}{2\beta}\left(e^{\beta(\mathbf{U}-\mathbf{I})}-e^{-\beta(\mathbf{U}-\mathbf{I})}\right). \tag{11}$$

As indicated by Peixoto et al. (2024), the scale function of the GHS-Hencky subfamily ($\gamma = 0$) is equal to the Itskov strain (Equation (4)). Following the notation of the Equation (1), the scale function of Equation (11) is

$$g(\lambda_i) = \frac{1}{2\beta}\left[e^{\beta(\lambda_i-1)}-e^{-\beta(\lambda_i-1)}\right]. \tag{12}$$

Figure 3 shows a plot of Equation (12) for certain values of β.

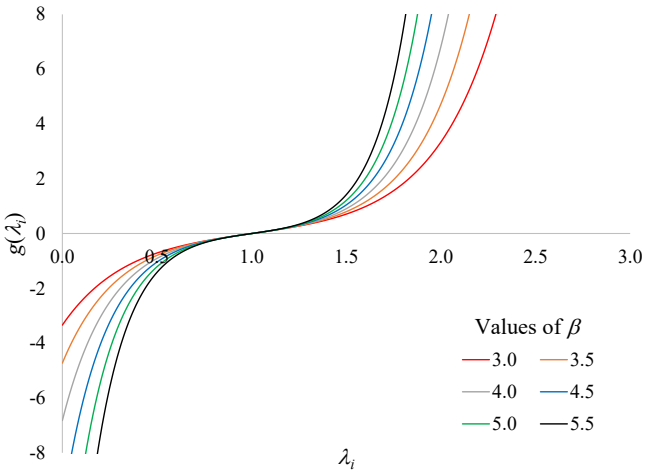

Figure 3 – GHS-Biot for some values of β.

From Figure 3, it can be concluded that similar behaviors in tension and compression are obtained for any value of β. However, requirement of the Equation $(2)_4$ does not hold. Nevertheless, during project development, the *strain range* that the materials can undergo is known. Therefore, by means of the parameter β, one can choose a material whose strain-stretching curve does not intercept the vertical axis within that range.

That said, this study has the following main objectives:

– to implement the GHS family considering $\gamma \in \mathbb{R}$ using the Positional Formulation of the Finite Element Method (PFFEM) and to perform 3D numerical simulations using the corresponding NGHL of the GHS-Biot strain tensor stated in Equation (11). Even though we focused on the GHS-Biot strain, the numerical implementation is quite general as we consider $\gamma \in \mathbb{R}$.

– to discuss the results and applicability of the proposed strain measure (Equation (11)).

2 PFFEM FOR AN ARBITRARY STRESS-STRAIN PAIR

The PFFEM was conceived approximately 20 years ago and has been shown to be reliable and accurate, as can be seen in Coda & Greco (2004) and Greco & Coda (2006). Its use with some classical hyperelastic models can be seen, e. g., in Santos et al. (2024). While the classical formulation of the FEM adopts linear nodal displacements as unknown variables, the PFFEM uses nodal positions. In this study, 3D analyses were performed using an eight-node hexahedral finite element with eight Gauss points. The usual mappings concerning a 3D computational implementation in the PFFEM context can be found, for example, in Coda & Paccola (2007) and are shown in Figure 4, where ξ, η, and ζ represent the fictitious space. Mappings $\boldsymbol{\chi}$ (reference configuration $\rightarrow$ current configuration), $\widetilde{\boldsymbol{\chi}}$ (fictitious space $\rightarrow$ current configuration) and $\overline{\boldsymbol{\chi}}$ (fictitious space $\rightarrow$ reference configuration) are defined such that $\boldsymbol{\chi} = \widetilde{\boldsymbol{\chi}} \circ \overline{\boldsymbol{\chi}}^{-1}$.

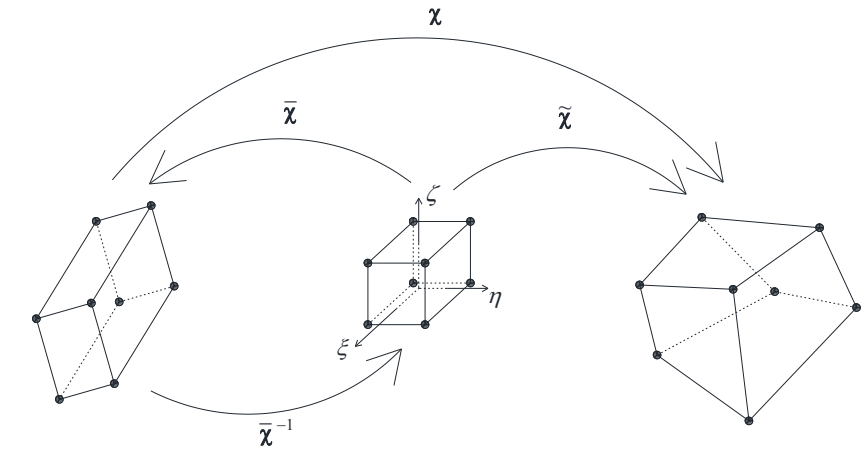

Figure 4 – Mappings concerning to a 3D computational implementation.

According to Coda & Paccola (2007),

$$\mathbf{F} = \widetilde{\mathbf{F}}\,\overline{\mathbf{F}}^{-1}, \tag{13}$$

where $\mathbf{F}$, $\widetilde{\mathbf{F}}$, and $\overline{\mathbf{F}}$ are the gradients of $\boldsymbol{\chi}$, $\widetilde{\boldsymbol{\chi}}$, and $\overline{\boldsymbol{\chi}}$, respectively. The total potential energy Π of a finite element is given by

$$\Pi = \int_{V_0} \psi \, dV_0 - f_a x_a, \qquad a = 1, 2, 3, \ldots, 24 \tag{14}$$

where ψ and V_0 are the strain energy density and initial volume, respectively, with respect to the reference configuration. The term f_a represents the force acting in the current nodal direction x_a. The equilibrium equation for an arbitrary Lagrangian work conjugate stress-strain pair ($\mathbf{T}$, $\mathbf{E}$) is obtained by differentiating Equation (14) with respect to x_a,

$$\frac{\partial \Pi}{\partial x_a} = 0 \Rightarrow \int_{V_0} \frac{\partial \psi}{\partial x_a} dV_0 - f_a = 0 \Rightarrow \int_{V_0} \frac{\partial \psi}{\partial E_{k\ell}} \frac{\partial E_{k\ell}}{\partial x_a} dV_0 - f_a = 0 \overset{\text{(I)}}{\Rightarrow} \int_{V_0} T_{k\ell} \frac{\partial E_{k\ell}}{\partial x_a} dV_0 - f_a = 0 \overset{\text{(II)}}{\Rightarrow}$$

$$\overset{\text{(II)}}{\Rightarrow} \int_{V_0} \left(2\mu E_{k\ell} + \lambda \delta_{k\ell} \operatorname{tr}\mathbf{E}\right) \frac{\partial E_{k\ell}}{\partial x_a} dV_0 - f_a = 0. \tag{15}$$

In step (I) we used the definition of hyperelasticity, $T_{k\ell} = \partial \psi / \partial E_{k\ell}$, and in step (II) we applied the NGHL, $T_{k\ell} = 2\mu E_{k\ell} + \lambda \, \delta_{k\ell} \operatorname{tr}\mathbf{E}$, where μ and λ are the Lamé parameters, and $\delta_{k\ell}$ is the Kronecker delta. Now, the expression $\partial E_{k\ell}/\partial x_a$ in Equation (15) is developed as

$$\frac{\partial E_{k\ell}}{\partial x_a} = \frac{\partial E_{k\ell}}{\partial F_{mn}} \frac{\partial F_{mn}}{\partial x_a} \overset{\text{(I)}}{=} \frac{\partial E_{k\ell}}{\partial F_{mn}} \frac{\partial \left(\widetilde{F}_{mq} \overline{F}^{-1}_{qn}\right)}{\partial x_a} \overset{\text{(II)}}{=} \frac{\partial E_{k\ell}}{\partial F_{mn}} \frac{\partial \widetilde{F}_{mq}}{\partial x_a} \overline{F}^{-1}_{qn}, \tag{16}$$

where in (I) we used Equation (13) and in (II) we applied the result $\partial \overline{F}^{-1}_{qn}/\partial x_a = 0$, as it can be noted from Figure 4. Next, from Equation (15) we define

$$h_a(\mathbf{x}) = \int_{V_0} \left(2\mu E_{k\ell} + \lambda \delta_{k\ell} \operatorname{tr}\mathbf{E}\right) \frac{\partial E_{k\ell}}{\partial x_a} dV_0 - f_a, \tag{17}$$

as components of the residual vector $\mathbf{h}(\mathbf{x})$. By differentiating Equation (17) with respect to x_b, we obtain the indicial notation of the Hessian $\nabla\mathbf{h}(\mathbf{x}_0)$,

$$\frac{\partial h_a}{\partial x_b} = \int_{V_0} \left(\left(2\mu \frac{\partial E_{k\ell}}{\partial x_b} + \lambda \delta_{k\ell} \left(\frac{\partial E_{11}}{\partial x_b} + \frac{\partial E_{22}}{\partial x_b} + \frac{\partial E_{33}}{\partial x_b} \right) \right) \frac{\partial E_{k\ell}}{\partial x_a} + T_{k\ell} \frac{\partial^2 E_{k\ell}}{\partial x_a \partial x_b} \right) dV_0. \qquad b = 1, 2, 3, \ldots, 24 \tag{18}$$

Now, let $\mathbf{h}(\mathbf{x}_0)$ and $\nabla\mathbf{h}(\mathbf{x}_0)$ be the residual vector and Hessian of the model regarding only unknown degrees of freedom (DOFs), respectively. Because the solution to the problem is the root of $\mathbf{h}(\mathbf{x})$, the Newton-Raphson scheme was used. Thus, by linearizing $\mathbf{h}(\mathbf{x})$ around a known vector $\mathbf{x}_0$, we obtain

$$\mathbf{h}(\mathbf{x}_0)+\nabla\mathbf{h}(\mathbf{x}_0)\Delta\mathbf{x}\cong\mathbf{0}\Rightarrow\Delta\mathbf{x}\cong-\nabla\mathbf{h}(\mathbf{x}_0)^{-1}\mathbf{h}(\mathbf{x}_0), \tag{19}$$

where $\Delta\mathbf{x}$ is the incremental position vector for only the unknown DOFs and $\mathbf{0}$ is the null vector. For a predefined tolerance *tol*, the convergence of the Newton-Raphson procedure is verified by $\|\Delta\mathbf{x}\|/\|\mathbf{x}\|\leq tol$, in which $\mathbf{x}=\mathbf{x}_0+\Delta\mathbf{x}$. Expression $\partial^2E_{k\ell}/\partial x_a\partial x_b$ of Equation (18) takes the form

$$\frac{\partial^2E_{k\ell}}{\partial x_a\partial x_b}=\frac{\partial}{\partial x_b}\left(\frac{\partial E_{k\ell}}{\partial F_{mn}}\frac{\partial\widetilde{F}_{mq}}{\partial x_a}\overline{F}^{-1}_{qn}\right)\overset{\text{(I)}}{=}\frac{\partial\widetilde{F}_{mq}}{\partial x_a}\overline{F}^{-1}_{qn}\frac{\partial}{\partial x_b}\left(\frac{\partial E_{k\ell}}{\partial F_{mn}}\right)=\frac{\partial\widetilde{F}_{mq}}{\partial x_a}\overline{F}^{-1}_{qn}\frac{\partial}{\partial F_{op}}\left(\frac{\partial E_{k\ell}}{\partial F_{mn}}\right)\frac{\partial F_{op}}{\partial x_b}\overset{\text{(II)}}{=}\frac{\partial\widetilde{F}_{mq}}{\partial x_a}\overline{F}^{-1}_{qn}\frac{\partial^2E_{k\ell}}{\partial F_{mn}\partial F_{op}}\frac{\partial\left(\widetilde{F}_{or}\overline{F}^{-1}_{rp}\right)}{\partial x_b}=$$

$$=\frac{\partial\widetilde{F}_{mq}}{\partial x_a}\overline{F}^{-1}_{qn}\frac{\partial\widetilde{F}_{or}}{\partial x_b}\overline{F}^{-1}_{rp}\frac{\partial^2E_{k\ell}}{\partial F_{mn}\partial F_{op}}, \tag{20}$$

where, in (I), we used the result $\partial^2\widetilde{F}_{mq}/\partial x_a\partial x_b=0$. In step (II), Equation (13) is applied. Thus, from Equations (16) and (20), it can be concluded that the PFFEM is completely determined if the derivatives $\partial E_{k\ell}/\partial F_{mn}$ and $\partial^2E_{k\ell}/\partial F_{mn}\partial F_{op}$ of the chosen strain tensor $\mathbf{E}$ are known. A nonexhaustive pseudocode of the program is shown in Figure 5a, where *incr*, *nincr*, *elem,* and *nelem* represent the increment, number of increments, element, and number of elements, respectively. The function `compute_ElemHessIntForce`(*elem*), which is responsible for calculating $\mathbf{h}(\mathbf{x}_j)$ and $\nabla\mathbf{h}(\mathbf{x}_j)$ for *elem*, is shown in Figure 5b, where *GP* and *nGP* represent the Gauss point and number of Gauss points, respectively.

```
START
read input
j = 0
for each incr in nincr {
   do{
      for each elem in nelem {
         function compute_ElemHessIntForce(elem)
         assemble h(x_j) and ∇h(x_j) to model
      }
      Δx_j = −∇h(x_j)^−1 h(x_j)
      x_{j+1} = x_j + Δx_j
      rnorm = ||Δx_j|| / ||x_{j+1}||
      j = j + 1
   } while (rnom > tol)
}
END
```

(a)

```
function compute_ElemHessIntForce(elem){
   for each GP in nGP{
      compute F̃, F̄ and F
      compute E and T
      compute dF̃/dx
      compute dE/dF
      compute dE/dx
      compute h(x_j)
      compute d²E/dF²
      compute d²E/dFdx
      compute d²E/dx²
      compute ∇h(x_j)
   }
}
```

(b)

Figure 5 – (a) Pseudo-code of the program. (b) Pseudo-code of the function `compute_ElemHessIntForce`(*elem*).

3 DERIVATIVES OF THE GHS STRAIN TENSOR WITH RESPECT TO THE DEFORMATION GRADIENT

In the following, we present the indicial expressions of the first and second derivatives of ${}^{\text{hs}}\mathbf{E}^{(\beta)}$ with respect to the deformation gradient $\mathbf{F}$ on a basis formed by the unit vectors along the axes of the Cartesian coordinate system (global directions), instead of on a basis formed by the eigenvectors of $\mathbf{U}$ and/or $\mathbf{V}$, where $\mathbf{V}$ is the left stretch tensor. This avoids

changes in the basis of the fourth- and sixth-order tensors in the code. The expressions $\partial\,{}^{\text{hs}}\mathbf{E}^{(\beta)}/\partial\mathbf{F}$ and $\partial^2\,{}^{\text{hs}}\mathbf{E}^{(\beta)}/\partial\mathbf{F}^2$ developed here do not make explicit use of $\partial\mathbf{U}/\partial\mathbf{F}$ (see Wheeler & Casey (2011)), and consequently neither of $\partial^2\mathbf{U}/\partial\mathbf{F}^2$.

Furthermore, one also shows how the Cauchy stress tensor $\mathbf{T}$ was calculated from the work conjugate stress tensor of ${}^{\text{hs}}\mathbf{E}^{(\beta)}$. Lastly, all functions of second-order tensors are computationally performed according to Mal & Singh (1991), i.e., $[\mathbf{G}(\mathbf{U})] = [{}_{\text{U}}\mathbf{Q}]\,[\mathbf{G}({}_{\text{U}}\mathbf{\Lambda})]\,[{}_{\text{U}}\mathbf{Q}]^{\text{T}}$, where $[{}_{\text{U}}\mathbf{Q}]$ is the orthogonal matrix whose columns are the normalized eigenvectors ($\boldsymbol{\alpha}_i$) of $\mathbf{U}$, and $[\mathbf{G}({}_{\text{U}}\mathbf{\Lambda})] = \text{diag}[g(\lambda_1), g(\lambda_2), g(\lambda_3)]$.

3.1 GHS's derivatives for $\gamma \neq 0$

Substituting Equation $(10)_1$ in Equation (9) one has

$$ {}^{\text{hs}}\mathbf{E}^{(\beta)} = \frac{1}{\beta}\sinh\left(\frac{\beta}{\gamma}(\mathbf{U}^{\gamma}-\mathbf{I})\right). \qquad (\beta \in \mathbb{R}^{*}_{+} \text{ and } \gamma \in \mathbb{R}^{*}) \tag{21} $$

Because γ is quite general, the determination of $\partial\,{}^{\text{hs}}E^{(\beta)}_{k\ell}/\partial F_{mn}$ may be laborious. However, one can use the logarithm properties, that is, $\mathbf{U}^{\gamma} = e^{\ln \mathbf{U}^{\gamma}} = e^{\gamma \ln \mathbf{U}}$. Thus, Equation (21) becomes

$$ {}^{\text{hs}}\mathbf{E}^{(\beta)} = \frac{1}{\beta}\sinh\left(\frac{\beta}{\gamma}(e^{\gamma\ln\mathbf{U}}-\mathbf{I})\right) = \frac{1}{2\beta}\left(\left(e^{\frac{\beta}{\gamma}(e^{\gamma\ln\mathbf{U}}-\mathbf{I})}\right)-\left(e^{-\frac{\beta}{\gamma}(e^{\gamma\ln\mathbf{U}}-\mathbf{I})}\right)\right). \tag{22} $$

The indicial notation of Equation (22) reads

$$ {}^{\text{hs}}E^{(\beta)}_{k\ell} = \frac{1}{2\beta}\left(\left(e^{\frac{\beta}{\gamma}(e^{\gamma\ln\mathbf{U}}-\mathbf{I})}\right)_{k\ell}-\left(e^{-\frac{\beta}{\gamma}(e^{\gamma\ln\mathbf{U}}-\mathbf{I})}\right)_{k\ell}\right). \tag{23} $$

Now, by defining $\mathbf{Z} = e^{\alpha\mathbf{X}}$ ($\alpha \in \mathbb{R}$), we can easily obtain

$$ \frac{\partial Z_{k\ell}}{\partial X_{mn}} = \alpha\,\delta_{\ell n}(e^{\alpha\mathbf{X}})_{km}. \tag{24} $$

Next, using the chain rule, we derive Equation (23) with respect to F_{mn} to obtain

$$ \frac{\partial\,{}^{\text{hs}}E^{(\beta)}_{k\ell}}{\partial F_{mn}} = \frac{1}{2\beta}\left(\frac{\partial\left(e^{\frac{\beta}{\gamma}(e^{\gamma\ln\mathbf{U}}-\mathbf{I})}\right)_{k\ell}}{\partial(e^{\gamma\ln\mathbf{U}}-\mathbf{I})_{st}}\frac{\partial(e^{\gamma\ln\mathbf{U}}-\mathbf{I})_{st}}{\partial(\ln\mathbf{U})_{uv}}\frac{\partial(\ln\mathbf{U})_{uv}}{\partial F_{mn}} - \frac{\partial\left(e^{-\frac{\beta}{\gamma}(e^{\gamma\ln\mathbf{U}}-\mathbf{I})}\right)_{k\ell}}{\partial(e^{\gamma\ln\mathbf{U}}-\mathbf{I})_{st}}\frac{\partial(e^{\gamma\ln\mathbf{U}}-\mathbf{I})_{st}}{\partial(\ln\mathbf{U})_{uv}}\frac{\partial(\ln\mathbf{U})_{uv}}{\partial F_{mn}}\right) \overset{\text{(I)}}{=} $$

$$ \overset{\text{(I)}}{=} \frac{1}{2\beta}\gamma\,\delta_{tv}(e^{\gamma\ln\mathbf{U}})_{su}\frac{\partial(\ln\mathbf{U})_{uv}}{\partial F_{mn}}\left(\frac{\beta}{\gamma}\delta_{\ell t}\left(e^{\frac{\beta}{\gamma}(e^{\gamma\ln\mathbf{U}}-\mathbf{I})}\right)_{ks}+\frac{\beta}{\gamma}\delta_{\ell t}\left(e^{-\frac{\beta}{\gamma}(e^{\gamma\ln\mathbf{U}}-\mathbf{I})}\right)_{ks}\right) \Rightarrow $$

$$ \Rightarrow \frac{\partial\,{}^{\text{hs}}E^{(\beta)}_{k\ell}}{\partial F_{mn}} = U^{\gamma}_{su}\frac{\partial(\ln\mathbf{U})_{u\ell}}{\partial F_{mn}}\left(\cosh\left(\frac{\beta}{\gamma}(\mathbf{U}^{\gamma}-\mathbf{I})\right)\right)_{ks}, \tag{25} $$

where in (I) we used Equation (24). Furthermore, by differentiating Equation (25) with respect to F_{op} using the product rule, we obtain

$$ \frac{\partial^2\,{}^{\text{hs}}E^{(\beta)}_{k\ell}}{\partial F_{mn}\partial F_{op}} = \frac{\partial(e^{\gamma\ln\mathbf{U}})_{su}}{\partial F_{op}}\frac{\partial(\ln\mathbf{U})_{u\ell}}{\partial F_{mn}}\left(\cosh\left(\frac{\beta}{\gamma}(\mathbf{U}^{\gamma}-\mathbf{I})\right)\right)_{ks} + U^{\gamma}_{su}\frac{\partial^2(\ln\mathbf{U})_{u\ell}}{\partial F_{mn}\partial F_{op}}\left(\cosh\left(\frac{\beta}{\gamma}(\mathbf{U}^{\gamma}-\mathbf{I})\right)\right)_{ks} + $$

$$+U^{\gamma}_{su}\frac{\partial(\ln\mathbf{U})_{u\ell}}{\partial F_{mn}}\frac{\partial}{\partial F_{op}}\left(\cosh\left(\frac{\beta}{\gamma}(\mathbf{U}^{\gamma}-\mathbf{I})\right)\right)_{ks}\overset{\text{(I)}}{=}$$

$$\overset{\text{(I)}}{=}\frac{\partial(e^{\gamma\ln\mathbf{U}})_{su}}{\partial(\ln\mathbf{U})_{wx}}\frac{\partial(\ln\mathbf{U})_{wx}}{\partial F_{op}}\frac{\partial(\ln\mathbf{U})_{u\ell}}{\partial F_{mn}}\left(\cosh\left(\frac{\beta}{\gamma}(\mathbf{U}^{\gamma}-\mathbf{I})\right)\right)_{ks}+U^{\gamma}_{su}\frac{\partial^2(\ln\mathbf{U})_{u\ell}}{\partial F_{mn}\partial F_{op}}\left(\cosh\left(\frac{\beta}{\gamma}(\mathbf{U}^{\gamma}-\mathbf{I})\right)\right)_{ks}+$$

$$+\frac{U^{\gamma}_{su}}{2}\frac{\partial(\ln\mathbf{U})_{u\ell}}{\partial F_{mn}}\left(\frac{\partial\left(e^{\frac{\beta}{\gamma}(e^{\gamma\ln\mathbf{U}}-\mathbf{I})}\right)_{ks}}{\partial(e^{\gamma\ln\mathbf{U}}-\mathbf{I})_{wx}}\frac{\partial(e^{\gamma\ln\mathbf{U}}-\mathbf{I})_{wx}}{\partial(\ln\mathbf{U})_{yz}}\frac{\partial(\ln\mathbf{U})_{yz}}{\partial F_{op}}+\frac{\partial\left(e^{-\frac{\beta}{\gamma}(e^{\gamma\ln\mathbf{U}}-\mathbf{I})}\right)_{ks}}{\partial(e^{\gamma\ln\mathbf{U}}-\mathbf{I})_{wx}}\frac{\partial(e^{\gamma\ln\mathbf{U}}-\mathbf{I})_{wx}}{\partial(\ln\mathbf{U})_{yz}}\frac{\partial(\ln\mathbf{U})_{yz}}{\partial F_{op}}\right)\overset{\text{(II)}}{=}$$

$$\overset{\text{(II)}}{=}\gamma\,\delta_{ux}(e^{\gamma\ln\mathbf{U}})_{sw}\frac{\partial(\ln\mathbf{U})_{wx}}{\partial F_{op}}\frac{\partial(\ln\mathbf{U})_{u\ell}}{\partial F_{mn}}\left(\cosh\left(\frac{\beta}{\gamma}(\mathbf{U}^{\gamma}-\mathbf{I})\right)\right)_{ks}+U^{\gamma}_{su}\frac{\partial^2(\ln\mathbf{U})_{u\ell}}{\partial F_{mn}\partial F_{op}}\left(\cosh\left(\frac{\beta}{\gamma}(\mathbf{U}^{\gamma}-\mathbf{I})\right)\right)_{ks}+$$

$$+\frac{U^{\gamma}_{su}}{2}\frac{\partial(\ln\mathbf{U})_{u\ell}}{\partial F_{mn}}\gamma\,\delta_{xz}(e^{\gamma\ln\mathbf{U}})_{wy}\frac{\partial(\ln\mathbf{U})_{yz}}{\partial F_{op}}\left(\frac{\beta}{\gamma}\delta_{sx}\left(e^{\frac{\beta}{\gamma}(e^{\gamma\ln\mathbf{U}}-\mathbf{I})}\right)_{kw}+\left(-\frac{\beta}{\gamma}\right)\delta_{sx}\left(e^{-\frac{\beta}{\gamma}(e^{\gamma\ln\mathbf{U}}-\mathbf{I})}\right)_{kw}\right)\Rightarrow$$

$$\Rightarrow\frac{\partial^2\,{}^{\text{hs}}E^{(\beta)}_{k\ell}}{\partial F_{mn}\partial F_{op}}=\gamma U^{\gamma}_{sw}\frac{\partial(\ln\mathbf{U})_{wu}}{\partial F_{op}}\frac{\partial(\ln\mathbf{U})_{u\ell}}{\partial F_{mn}}\left(\cosh\left(\frac{\beta}{\gamma}(\mathbf{U}^{\gamma}-\mathbf{I})\right)\right)_{ks}+U^{\gamma}_{su}\frac{\partial^2(\ln\mathbf{U})_{u\ell}}{\partial F_{mn}\partial F_{op}}\left(\cosh\left(\frac{\beta}{\gamma}(\mathbf{U}^{\gamma}-\mathbf{I})\right)\right)_{ks}+$$

$$+\beta U^{\gamma}_{su}U^{\gamma}_{wy}\frac{\partial(\ln\mathbf{U})_{u\ell}}{\partial F_{mn}}\frac{\partial(\ln\mathbf{U})_{ys}}{\partial F_{op}}\left(\sinh\left(\frac{\beta}{\gamma}(\mathbf{U}^{\gamma}-\mathbf{I})\right)\right)_{kw},\qquad(26)$$

where in (I), the chain rule is used, and Equation (24) is applied in (II). The indicial expressions of $\partial(\ln\mathbf{U})/\partial\mathbf{F}$ and $\partial^2(\ln\mathbf{U})/\partial\mathbf{F}^2$ in Equations (25) and (26) written directly in the global direction have not been found in the literature; therefore, they are given in Appendix A.

Now, let ${}^{\text{hs}}\mathbf{T}^{(\beta)}$ be the work conjugate stress tensor of ${}^{\text{hs}}\mathbf{E}^{(\beta)}$. Further, let ${}^{f}\mathbf{E}=f(\lambda_i)\,(\boldsymbol{\alpha}_i\otimes\boldsymbol{\alpha}_i)$ and ${}^{g}\mathbf{E}=g(\lambda_i)\,(\boldsymbol{\alpha}_i\otimes\boldsymbol{\alpha}_i)$ be arbitrary Lagrangian strain tensors and let ${}^{f}\mathbf{T}={}^{f}\overline{T}_{ij}\,(\boldsymbol{\alpha}_i\otimes\boldsymbol{\alpha}_j)$ and ${}^{g}\mathbf{T}={}^{g}\overline{T}_{ij}\,(\boldsymbol{\alpha}_i\otimes\boldsymbol{\alpha}_j)$ be their work conjugate stress tensors, respectively. The over bar ($\overline{\ }$) indicates the stress components of the corresponding stress tensor written in the $\{\boldsymbol{\alpha}_i\}$ basis. For non-coalescent principal stretches, one gets by Farahani & Naghdabadi (2003)

$$\begin{cases}{}^{f}\overline{T}_{ii}=\dfrac{g'(\lambda_i)}{f'(\lambda_i)}\,{}^{g}\overline{T}_{ii} & i=1,2,3\\ {}^{f}\overline{T}_{ij}=\dfrac{g(\lambda_i)-g(\lambda_j)}{f(\lambda_i)-f(\lambda_j)}\,{}^{g}\overline{T}_{ij} & i\neq j\end{cases}.\qquad\text{(no sum over repeated indices)}\qquad(27)$$

Setting in Equation (27) $f(\lambda_i)=(\lambda_i^2-1)/2$, which is the Green strain, and $g(\lambda_i)=(1/\beta)\sinh[(\beta/\gamma)(\lambda_i^{\gamma}-1)]$, which is the scale function of the Equation (21), we obtain

$$\begin{cases} \overline{S}_{ii} = \lambda_i^{\gamma-2}\cosh\left[\dfrac{\beta}{\gamma}\left(\lambda_i^{\gamma}-1\right)\right]\,{}^{\text{hs}}\overline{T}_{ii}^{(\beta)} & i=1,2,3 \\ \overline{S}_{ij} = \dfrac{2}{\beta}\dfrac{\sinh\left[\dfrac{\beta}{\gamma}\left(\lambda_i^{\gamma}-1\right)\right]-\sinh\left[\dfrac{\beta}{\gamma}\left(\lambda_j^{\gamma}-1\right)\right]}{\lambda_i^2-\lambda_j^2}\,{}^{\text{hs}}\overline{T}_{ij}^{(\beta)} & i\neq j \end{cases}, \quad \text{(no sum over repeated indices)} \tag{28}$$

where $\mathbf{S}$ is the second Piola-Kirchhoff stress tensor. Thus, the Cauchy stress is found as follows. After calculating ${}^{\text{hs}}\overline{T}_{ij}^{(\beta)}$ using the NGHL, we use Equation (28). Next, one employs $[S_{ij}] = [_{\mathbf{U}}\mathbf{Q}]\,[\overline{S}_{ij}]\,[_{\mathbf{U}}\mathbf{Q}]^{\mathsf{T}}$. Once $\mathbf{S}$ was obtained in the global direction, $\mathbf{T}$ was computed using $\mathbf{T} = (\det\mathbf{F})^{-1}\,\mathbf{F}\mathbf{S}\mathbf{F}^{\mathsf{T}}$.

Expressions regarding Equation (27) for the case of coalescent principal stretches were taken directly from Farahani & Naghdabadi (2003) and are not given here.

3.2 GHS's derivatives for $\gamma = 0$

Substituting Equation $(10)_2$ in Equation (9) one has

$${}^{\text{hs}}\mathbf{E}^{(\beta)} = \frac{1}{\beta}\sinh(\beta\ln\mathbf{U}) = \frac{1}{2\beta}\left(\mathbf{U}^{\beta}-\mathbf{U}^{-\beta}\right) \quad \text{or} \quad {}^{\text{hs}}E_{k\ell}^{(\beta)} = \frac{1}{2\beta}\left(U_{k\ell}^{\beta}-U_{k\ell}^{-\beta}\right). \qquad (\beta\in\mathbb{R}_+^*) \tag{29}$$

Using the same logarithm properties applied in the previous item, Equation $(29)_2$ becomes

$${}^{\text{hs}}E_{k\ell}^{(\beta)} = \frac{1}{2\beta}\left((e^{\beta\ln\mathbf{U}})_{k\ell}-(e^{-\beta\ln\mathbf{U}})_{k\ell}\right). \tag{30}$$

Now, using the chain rule on Equation (30) one gets

$$\frac{\partial\,{}^{\text{hs}}E_{k\ell}^{(\beta)}}{\partial F_{mn}} = \frac{1}{2\beta}\left(\frac{\partial(e^{\beta\ln\mathbf{U}})_{k\ell}}{\partial(\ln\mathbf{U})_{st}}\frac{\partial(\ln\mathbf{U})_{st}}{\partial F_{mn}}-\frac{\partial(e^{-\beta\ln\mathbf{U}})_{k\ell}}{\partial(\ln\mathbf{U})_{st}}\frac{\partial(\ln\mathbf{U})_{st}}{\partial F_{mn}}\right)\overset{\text{(I)}}{=}$$

$$\overset{\text{(I)}}{=}\frac{1}{2\beta}\frac{\partial(\ln\mathbf{U})_{st}}{\partial F_{mn}}\left(\beta\,\delta_{\ell t}(e^{\beta\ln\mathbf{U}})_{ks}+\beta\,\delta_{\ell t}(e^{-\beta\ln\mathbf{U}})_{ks}\right)\Rightarrow\frac{\partial\,{}^{\text{hs}}E_{k\ell}^{(\beta)}}{\partial F_{mn}} = \frac{1}{2}\frac{\partial(\ln\mathbf{U})_{s\ell}}{\partial F_{mn}}\left(U_{ks}^{\beta}+U_{ks}^{-\beta}\right). \tag{31}$$

where in (I) we used Equation (24). Differentiating Equation (31) with respect to F_{op}, we obtain

$$\frac{\partial^2\,{}^{\text{hs}}E_{k\ell}^{(\beta)}}{\partial F_{mn}\partial F_{op}} = \frac{1}{2}\left(\frac{\partial^2(\ln\mathbf{U})_{s\ell}}{\partial F_{mn}\partial F_{op}}\left(U_{ks}^{\beta}+U_{ks}^{-\beta}\right)+\frac{\partial(\ln\mathbf{U})_{s\ell}}{\partial F_{mn}}\left(\frac{\partial(e^{\beta\ln\mathbf{U}})_{ks}}{\partial(\ln\mathbf{U})_{uv}}\frac{\partial(\ln\mathbf{U})_{uv}}{\partial F_{op}}+\frac{\partial(e^{-\beta\ln\mathbf{U}})_{ks}}{\partial(\ln\mathbf{U})_{uv}}\frac{\partial(\ln\mathbf{U})_{uv}}{\partial F_{op}}\right)\right)\Rightarrow$$

$$\Rightarrow\frac{\partial^2\,{}^{\text{hs}}E_{k\ell}^{(\beta)}}{\partial F_{mn}\partial F_{op}} = \frac{1}{2}\left(\frac{\partial^2(\ln\mathbf{U})_{s\ell}}{\partial F_{mn}\partial F_{op}}\left(U_{ks}^{\beta}+U_{ks}^{-\beta}\right)+\beta\frac{\partial(\ln\mathbf{U})_{s\ell}}{\partial F_{mn}}\frac{\partial(\ln\mathbf{U})_{us}}{\partial F_{op}}\left(U_{ku}^{\beta}-U_{ku}^{-\beta}\right)\right). \tag{32}$$

Now, setting in Equation (27) $f(\lambda_i)$ as the Green strain and $g(\lambda_i) = (\lambda_i^{\beta} - \lambda_i^{-\beta})/2\beta$, we obtain

$$\begin{cases} \overline{S}_{ii} = \dfrac{\lambda_i^{\beta-1} + \lambda_i^{-\beta-1}}{2\lambda_i}\ {}^{\text{hs}}\overline{T}_{ii}^{(\beta)} & i = 1,2,3 \\ \overline{S}_{ij} = \dfrac{\lambda_i^{\beta} - \lambda_i^{-\beta} - \lambda_j^{\beta} + \lambda_j^{-\beta}}{\beta(\lambda_i^2 - \lambda_j^2)}\ {}^{\text{hs}}\overline{T}_{ij}^{(\beta)} & i \neq j \end{cases}, \quad \text{(no sum over repeated indices)} \tag{33}$$

and, similar to the previous item, one computes $\mathbf{T}$.

4 NUMERICAL APPLICATIONS

In the following, a nonlinear analysis is performed in examples 4.1, 4.2 and 4.4 (non-isochoric deformation) with a fixed increment load Δq using the Newton-Raphson scheme. Only in example 4.3 (isochoric deformation) are all the positions prescribed in each step. Finally, a comparison of the analytical and numerical results with the data from Zenkert & Burman (2009) is presented in example 4.5. Stresses in the nodes are obtained by the weighted arithmetic mean using the stresses of the Gauss points of finite elements having the corresponding node; the weight is the distance of each Gauss point to that node.

In this work, the Lamé parameters μ and λ are obtained from E and ν by widely known expressions, for example, on page 13 of Mal & Singh (1991). All examples adopted $\beta = 3.5$ and considered GHS-Biot strain, as shown in Figure 6.

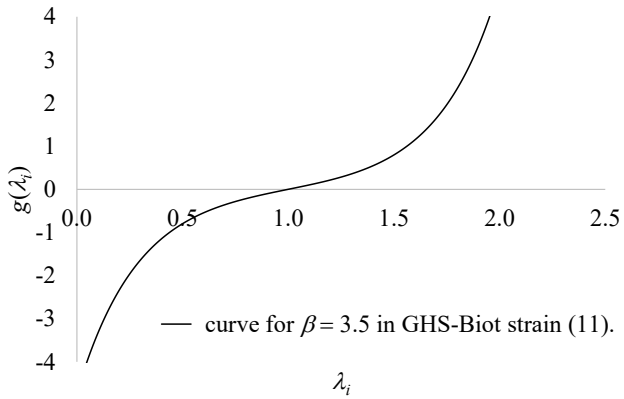

Figure 6 – Material strain curve used in the numerical examples.

4.1 Axial Problem (AP)

Figure 7a shows the uniformly distributed axial loading q of a prismatic solid with a square base (side: 1.0 m) and a height of 0.125 m. The two-plane symmetry of the problem was considered for modeling purposes, resulting in the mesh shown in Figure 7b. The following graphs are required for this problem: $T_{11}/\mu \times \lambda_1$ at point *A* (indicated in Figure 7b) and $\varepsilon_V \times \lambda_1$, where $\varepsilon_V = \Delta V / V_0$ is the volumetric strain of the model.

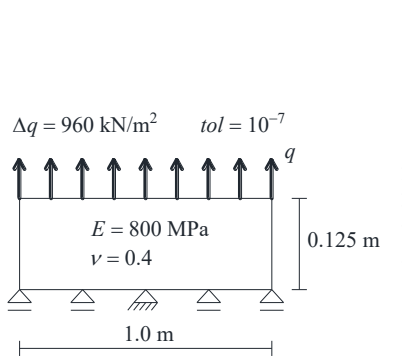

(a)

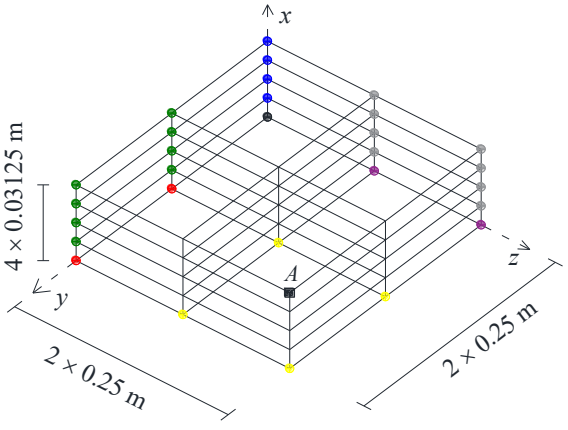

Nodes colors	Constraints (1 - restrained; 0 - free)		
	x	y	z
Black	1	1	1
Red	1	0	1
Green	0	0	1
Blue	0	1	1
Gray	0	1	0
Yellow	1	0	0
Purple	1	1	0

(b)

Figure 7 – (a) Axial problem data. (b) Mesh used (two-plane symmetry is applied).

According to Peixoto et al. (2024), the analytical formula of T_{11} for AP is

$$T_{11} = \frac{\omega}{\beta}\cosh\left[\beta(\lambda_1 - 1)\right]\sinh\left[\beta(\lambda_1 - 1)\right]\left\{\frac{1}{\beta}\operatorname{arcsinh}\left\{-\nu\sinh\left[\beta(\lambda_1 - 1)\right]\right\} + 1\right\}^{-2}, \tag{34}$$

where $\omega = \mu[(3\lambda + 2\mu)]/(\mu + \lambda)$. Further, the analytical volumetric strain for AP is

$$\varepsilon_{\not\vdash} = \lambda_1\left\{\frac{1}{\beta}\operatorname{arcsinh}\left\{-\nu\sinh\left[\beta(\lambda_1 - 1)\right]\right\} + 1\right\}^{2} - 1\,. \tag{35}$$

Thus, Figure 8 and Figure 9 show the required curves.

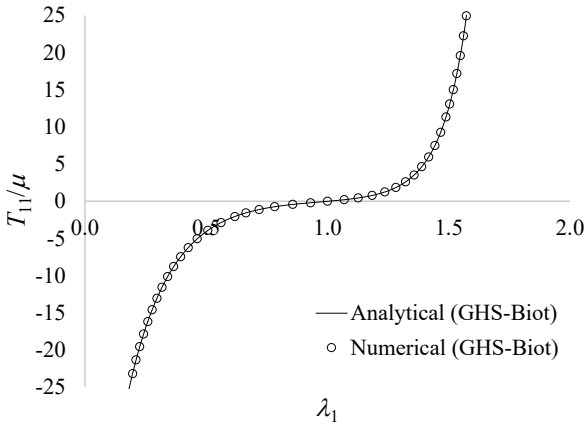

Figure 8 – Analytical and numerical T_{11} of point *A* of AP.

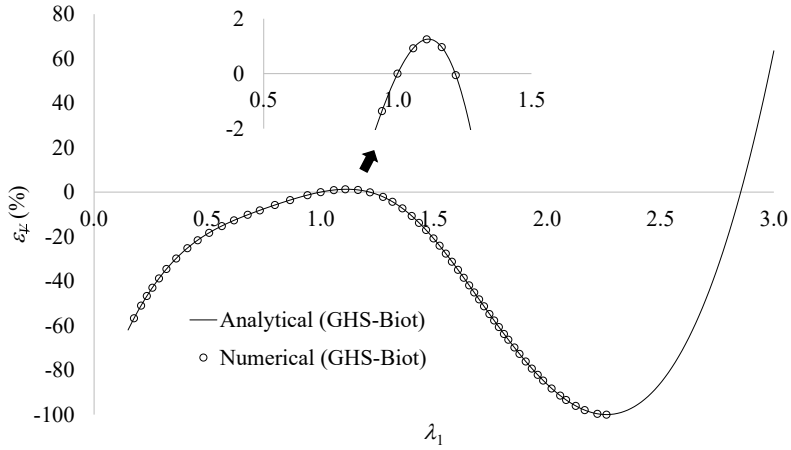

Figure 9 – Analytical and numerical volumetric strain of AP.

Figure 8 and Figure 9 show that the numerical responses fit the analytical responses well. Regarding the volumetric strain, in the compression regime ($\lambda_1 < 1$) the volume reduces as stretching approaches zero, whereas in the tension regime there is an initial volume increase, followed by a volume decrease. After $\lambda_1 \cong 2.26$, GHS-Biot exhibited a continuous volume increase, from which the computational code was unable to obtain numerical results.

4.2 Equi-Biaxial Problem (EBP)

Figure 10a shows the equibiaxial loading q of a cubic solid on the 0.05 m side. The three-plane symmetry of the problem was considered for modeling purposes, leading to a mesh with cubic finite elements on 6.25×10^{-3} m side (Figure 10b). The boundary conditions are shown in Figure 10c (external surfaces are not indicated). The following graphs were used for this problem: $T_{11}/\mu \times \lambda_1$ at point *A* (Figure 10a) and $\varepsilon_{\not\vdash} \times \lambda_1$.

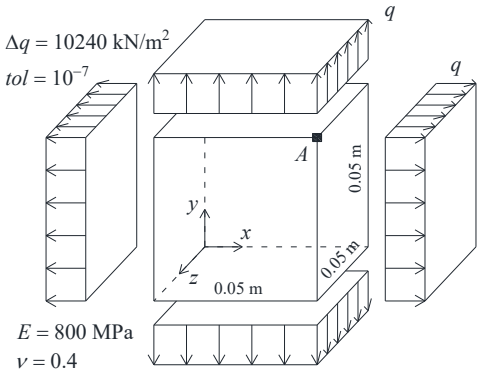

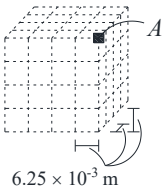

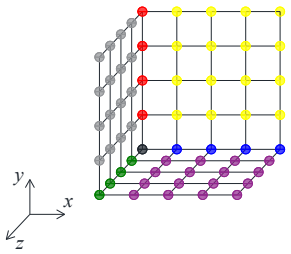

Nodes colors	Constraints (1 - restrained; 0 - free)		
	x	*y*	*z*
Black	1	1	1
Red	1	0	1
Green	1	1	0
Blue	0	1	1
Gray	1	0	0
Yellow	0	0	1
Purple	0	1	0

(a) (b) (c)

Figure 10 – (a) Equi-biaxial problem data. (b) Mesh used. (c) Boundary conditions.

According to Peixoto et al. (2024), the analytical formula of T_{11} for EBP is

$$T_{11} = \frac{\overline{\omega}}{\lambda_1 \beta} \cosh[\beta(\lambda_1 - 1)] \sinh[\beta(\lambda_1 - 1)] \left\{ \frac{1}{\beta} \operatorname{arcsinh}\left\{ \frac{2\nu}{\nu - 1} \sinh[\beta(\lambda_1 - 1)] \right\} + 1 \right\}^{-1}, \tag{36}$$

where $\overline{\omega} = 2\mu[(3\lambda + 2\mu)]/(2\mu + \lambda)$. Further, the analytical volumetric strain for EBP is

$$\varepsilon_v = \lambda_1^2 \left\{ \frac{1}{\beta} \operatorname{arcsinh}\left\{ \frac{2\nu}{\nu - 1} \sinh[\beta(\lambda_1 - 1)] \right\} + 1 \right\} - 1. \tag{37}$$

Figure 11 and Figure 12 present the required curves.

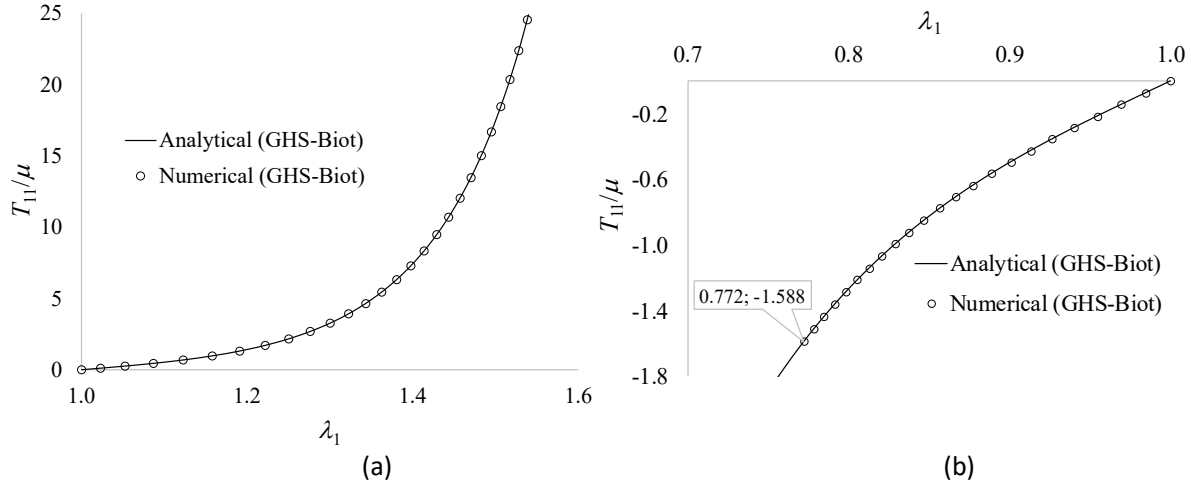

(a) (b)

Figure 11 – Analytical and numerical T_{11} of point *A* for EBP in (a) tension regime and (b) compression regime.

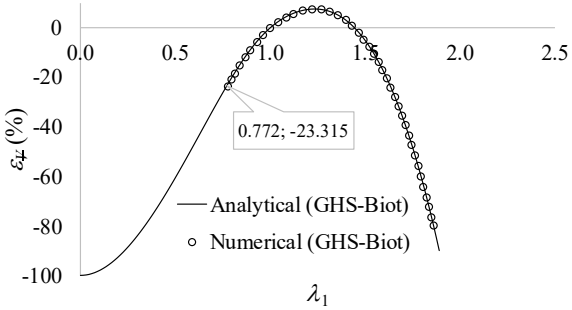

Figure 12 – Analytical and numerical volumetric strains for EBP.

According to Figure 11 and Figure 12, the numerical responses present a limitation in the compression regime, in contrast to the tension regime. The analysis stopped at approximately $\lambda_1 \cong 0.772$.

The volumetric strain decreased as the stretching approached zero (Figure 12). In the tension regime, GHS-Biot produced an initial increase in volume, followed by a continuous decrease.

4.3 Simple Shear in Plane Strain (SS-PStrain)

Figure 13a shows a prismatic solid with a base of 5 m × 2 m and a 1.0 m height. One-plane symmetry was considered for modeling purposes, resulting in the mesh shown in Figure 13b. The points in xz-plane at $y = 0$ were constrained in all directions, and the remaining points were constrained only in y- and z-directions. The following graph is required for this problem: $T_{12}/\mu \times \upsilon$ at point *A* (indicated in Figure 13b), which υ is defined in Figure 13a. In this example, the volumetric strain is zero because the SS-PStrain is an isochoric deformation.

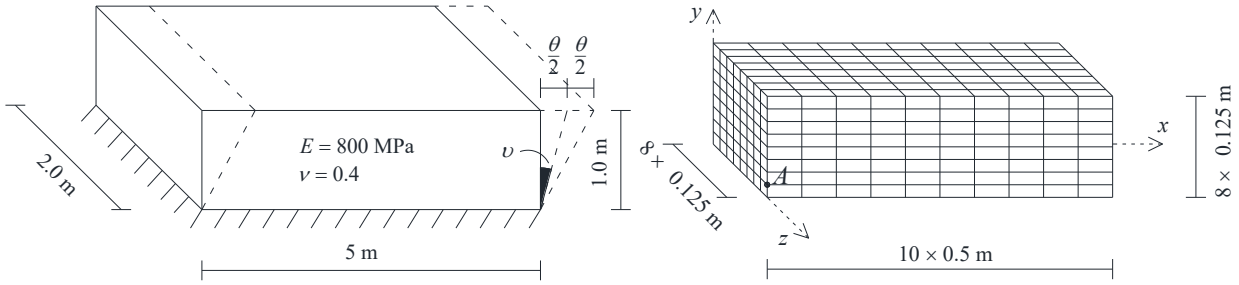

Figure 13 – (a) Data of simple shear in plane strain (b) Mesh used.

Because the analytical deformation gradient of SS-PStrain is

$$[\mathbf{F}] = \begin{bmatrix} 1 & \theta & 0 \\ 0 & 1 & 0 \\ 0 & 0 & 1 \end{bmatrix}, \tag{38}$$

we decided to manually update the x-coordinates of points out of the xz plane at $y = 0$ through analysis; thus, the numerical deformation gradient is equal to Equation (38) at any point in the model. This example is a simple verification and serves as the basis for the next one. The increment in x (Δx) in each step depends on the y-coordinate of the point, as shown in Table 1.

Table 1 – Increments in x-direction in simple shear in plane strain.

y-coordinate of the point (m)	Δx (m)
1.0	0.01
0.875	8.75×10^{-3}
0.75	7.5×10^{-3}
0.625	6.25×10^{-3}
0.5	5.0×10^{-3}
0.375	3.75×10^{-3}
0.25	2.5×10^{-3}
0.125	1.25×10^{-3}

According to Peixoto et al. (2024), the analytical formula of T_{12} for SS-PStrain is

$$T_{12} = \frac{1}{2\beta\lambda_1}\cosh[\beta(\lambda_1-1)][\cos\upsilon + \theta(1+\sin\upsilon)]\{2\mu\sinh[\beta(\lambda_1-1)] + \lambda\{\sinh[\beta(\lambda_1-1)] + \sinh[\beta(\lambda_2-1)]\}\} +$$

$$-\frac{1}{2\beta\lambda_2}\cosh[\beta(\lambda_2-1)][\cos\upsilon+\theta(\sin\upsilon-1)]\{2\mu\sinh[\beta(\lambda_2-1)]+\lambda\{\sinh[\beta(\lambda_1-1)]+\sinh[\beta(\lambda_2-1)]\}\}, \tag{39}$$

where $\upsilon = \text{arctg}(\theta/2)$ and $\lambda_1 = (1 + \sin\upsilon)/\cos\upsilon$, $\lambda_2 = (1 - \sin\upsilon)/\cos\upsilon$. Figure 14 shows the requested curve.

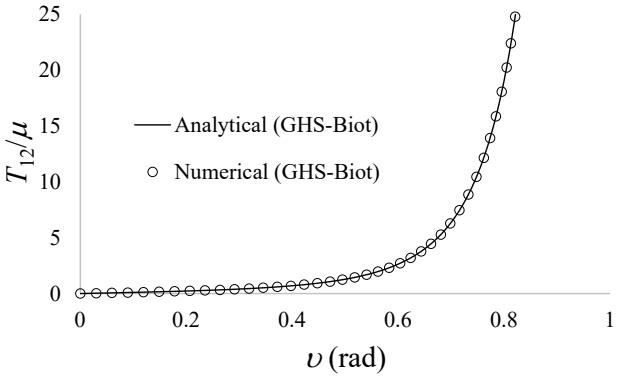

Figure 14 – Analytical and numerical T_{12} of point *A* for SS-PStrain.

From Figure 14, it can be concluded that the numerical responses fit excellently with the analytical responses, as expected.

4.4 Simple Shear in Plane Stress (SS-PStress)

The SS-PStress data are the same as those in the previous example, except for the boundary conditions. Figure 15 presents further details. The nodes not indicated in were restrained only in the y-direction. The following graphs are required for this problem: $T_{12}/\mu \times \upsilon$ for point *A* and $\varepsilon_{yy} \times \upsilon$.

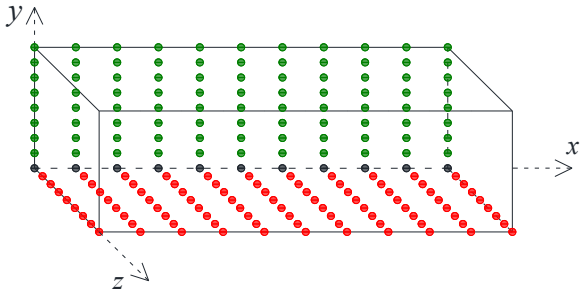

Nodes colors	Constraints (1 - restrained; 0 - free)		
	x	*y*	*z*
Black	1	1	1
Red	1	1	0
Green	0	1	1

Figure 15 – Boundary conditions in SS-PStress.

Because the analytical deformation gradient of SS-PStress is

$$[\mathbf{F}] = \begin{bmatrix} 1 & \theta & 0 \\ 0 & 1 & 0 \\ 0 & 0 & \lambda_3 \end{bmatrix}, \tag{40}$$

we decided to update the x-coordinates of the points out of the xz plane at $y = 0$ in the same manner as in the previous example. Now, z-coordinates of the points outside the xy plane at $z = 0$ become the degrees of freedom.

Considering Equation (40), we compute the analytical formula of T_{12} for SS-PStress as

$$T_{12} = \frac{1}{\lambda_3}\left\{\frac{1}{2\beta\lambda_1}\cosh[\beta(\lambda_1-1)][\cos\upsilon+\theta(1+\sin\upsilon)]\{2\mu\sinh[\beta(\lambda_1-1)]+\lambda\{\sinh[\beta(\lambda_1-1)]+\sinh[\beta(\lambda_2-1)]\}\}+\right.$$

$$-\frac{1}{2\beta\lambda_2}\cosh[\beta(\lambda_2-1)][\cos\upsilon+\theta(\sin\upsilon-1)]\{2\mu\sinh[\beta(\lambda_2-1)]+\lambda\{\sinh[\beta(\lambda_1-1)]+\sinh[\beta(\lambda_2-1)]\}\}, \tag{41}$$

where λ_1 and λ_2 are the same of the previous example and

$$\lambda_3=\frac{1}{\beta}\operatorname{arcsinh}\left\{-\frac{\lambda}{2\mu+\lambda}\{\sinh[\beta(\lambda_1-1)]+\sinh[\beta(\lambda_2-1)]\}\right\}+1\,. \tag{42}$$

Further, the analytical volumetric strain for SS-PStress is

$$\varepsilon_{\forall}=\frac{1}{\beta}\operatorname{arcsinh}\left\{\frac{-\lambda}{2\mu+\lambda}\{\sinh[\beta(\lambda_1-1)]+\sinh[\beta(\lambda_2-1)]\}\right\}. \tag{43}$$

Figure 16 and Figure 17 show the curves requested.

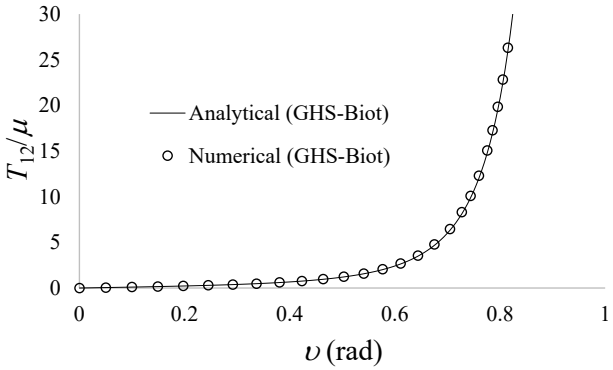

Figure 16 – Analytical and numerical T_{12} of the point *A* for SS-PStress.

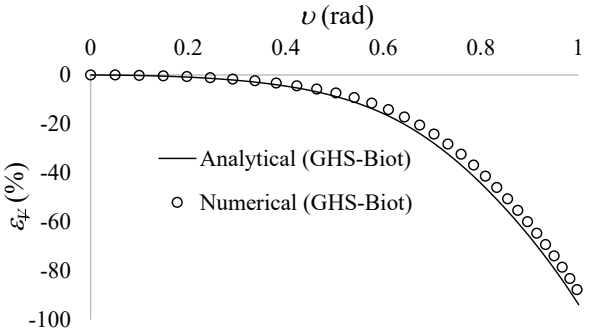

Figure 17 – Analytical and numerical volumetric strains for SS-PStress.

From Figure 16, the numerical T_{12} aligns significantly with the analytical T_{12}. Concerning the volumetric strain, as υ increased, a slight difference was observed between the numerical and analytical responses, as indicated in Figure 17.

4.5 Comparison with the data from Zenkert & Burman (2009)

In this example, we compare the proposed analytical and numerical models with the data from Zenkert & Burman (2009) for a closed cell rigid polymer foam in the axial problem. The samed data, mesh, and boundary conditions are those in Example 4.1 (Figure 7) are used, with the following exceptions: $E=367$ MPa and $\Delta q=320$ kN/m². The results are presented in Figure 18.

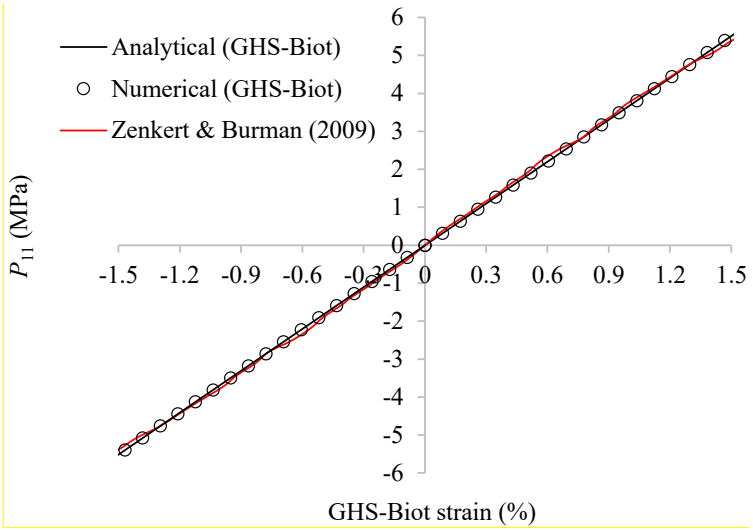

Figure 18 – Analytical and numerical results and Zenkert & Burman (2009)'s data.

According to Figure 18, the analytical and numerical results present a good fitting with the foam from Zenkert & Burman (2009). It is worth noting that the strain limit of 1.5 % (Figure 18) is higher than the typical practice by aerospace industry (0.4 % strain) for a different kind of polymer, based on carbon fiber epoxy matrix composites (Tsai & Melo, 2014).

5 CONCLUSIONS

Given that a material exhibits the same behavior in tension and compression on the stress-strain diagram (odd function), it is appropriate to incorporate a same behavior in tension and compression on the strain-stretching curve of this material. By idealizing a linear response on the stress-strain diagram for a given strain measure, the requirement of the scale function g to achieve the desired behavior on the strain-stretching curve is stated, which has been established in the Equation (6).

Owing to the strain measure (GHS-Biot) satisfying Equation (6), which also provides reasonable physical responses within a strain range, 3D numerical examples were used to demonstrate the applicability of the new Hooke-like constitutive model generated by this strain tensor. Besides, a comparison between the numerical and analytical responses and the data of a polymer foam from Zenkert & Burman (2009) was presented for the axial problem. The proposed model proved to be satisfactorily accurate within the 1.5% strain range. Although only GHS-Biot was tested in this work, the computational implementation presented is quite general because it considers $\gamma \in \mathbb{R}$ (see items 3.1 and 3.2) to obtain the derivatives of the strain tensors with respect to the deformation gradient, which have been written directly in global directions. The numerical results yielded an excellent correlation with the analytical responses in all three 3D examples analyzed (see items 4.1, 4.2 and 4.4). This demonstrates the precision and robustness of the developed formulation as well as its versatility.

This work shows that symmetry in tension and compression in both stress-strain and strain-stretching curves is numerically feasible using the GHS-Biot measure. Moreover, the presence of the parameter β expands the modeling options (see Figure 3) for a material with symmetry in the two aforementioned graphs. Concerning the volumetric strain, the GHS-Biot measure led to curious behaviors in the examples studied. This indicates that the GHS family is versatile, as it allows for the modeling of a compressible metamaterial possessing a singular behavior of volumetric strain.

This study opens many other fields of research. Using a decimal number γ in the code developed here, we expect to demonstrate the use of the GHS family to model biological tissues and biomaterials.

APPENDIX A

If $\{\mathbf{e}_i\}$ is the canonical basis of the Cartesian coordinate system (referential basis), then a second-order tensor $\mathbf{A}$ and a fourth-order tensor $\mathbf{A}$ are written as $\mathbf{A} = A_{ij}(\mathbf{e}_i \otimes \mathbf{e}_j)$ and $\mathbf{A} = A_{ijk\ell}(\mathbf{e}_i \otimes \mathbf{e}_j \otimes \mathbf{e}_k \otimes \mathbf{e}_\ell)$, respectively. The inner product ':' between two second-order tensors has the following properties

$$\mathbf{A}:(\mathbf{BV})=(\mathbf{B}^{\mathsf{T}}\mathbf{A}):\mathbf{V} \quad \text{and} \quad \mathbf{A}:(\mathbf{BCV})=(\mathbf{B}^{\mathsf{T}}\mathbf{AV}^{\mathsf{T}}):\mathbf{C}\,. \tag{44}$$

According to Holzapfel (2000), tensor product $\mathbf{A}\otimes\mathbf{B}$ is a fourth-order tensor such that

$$(\mathbf{A}\otimes\mathbf{B}):\mathbf{V}=(\mathbf{B}:\mathbf{V})\mathbf{A}\,. \tag{45}$$

Moreover, the properties

$$\mathbf{a}\otimes\mathbf{b}\otimes\mathbf{c}\otimes\mathbf{d}=(\mathbf{a}\otimes\mathbf{b})\otimes(\mathbf{c}\otimes\mathbf{d}) \quad \text{and} \quad (\mathbf{a}\otimes\mathbf{b})(\mathbf{c}\otimes\mathbf{d})=\mathbf{b}\cdot\mathbf{c}\,(\mathbf{a}\otimes\mathbf{d}) \tag{46}$$

will be useful. Next, following Holzapfel (2000), there are fourth-order unit tensors $\mathbf{I}$ and $\overline{\mathbf{I}}$ such that

$$\mathbf{A}=\mathbf{I}:\mathbf{A} \quad \text{and} \quad \mathbf{A}^{\mathsf{T}}=\overline{\mathbf{I}}:\mathbf{A}\,, \tag{47}$$

with

$$\mathbf{I}=I_{ijk\ell}(\mathbf{e}_i\otimes\mathbf{e}_j\otimes\mathbf{e}_k\otimes\mathbf{e}_\ell)=\delta_{ik}\delta_{j\ell}(\mathbf{e}_i\otimes\mathbf{e}_j\otimes\mathbf{e}_k\otimes\mathbf{e}_\ell) \quad \text{and} \quad \overline{\mathbf{I}}=\overline{I}_{ijk\ell}(\mathbf{e}_i\otimes\mathbf{e}_j\otimes\mathbf{e}_k\otimes\mathbf{e}_\ell)=\delta_{i\ell}\delta_{jk}(\mathbf{e}_i\otimes\mathbf{e}_j\otimes\mathbf{e}_k\otimes\mathbf{e}_\ell). \tag{48}$$

Now, as $\mathbf{U}=\sqrt{\mathbf{F}^{\mathsf{T}}\mathbf{F}}$, one defines $\mathbf{K}(\mathbf{F})=\ln(\sqrt{\mathbf{F}^{\mathsf{T}}\mathbf{F}})$. Applying the Gateaux differential (Itskov, 2019) to function $\mathbf{K}(\mathbf{F})$, we obtain

$$D\mathbf{K}(\mathbf{F})[\mathbf{A}]=\left.\frac{d\,\mathbf{K}(\mathbf{F}+\alpha\mathbf{A})}{d\alpha}\right|_{\alpha=0}=\left.\frac{d}{d\alpha}\left[\ln\sqrt{(\mathbf{F}+\alpha\mathbf{A})^{\mathsf{T}}(\mathbf{F}+\alpha\mathbf{A})}\right]\right|_{\alpha=0}=\frac{1}{2}(\mathbf{F}^{\mathsf{T}}\mathbf{F})^{-1}(\mathbf{F}^{\mathsf{T}}\mathbf{A}+\mathbf{A}^{\mathsf{T}}\mathbf{F})\Rightarrow$$

$$\Rightarrow D\mathbf{K}(\mathbf{F})[\mathbf{A}]=\frac{1}{2}(\mathbf{F}^{-1}\mathbf{A}+\mathbf{F}^{-1}\mathbf{F}^{-\mathsf{T}}\mathbf{A}^{\mathsf{T}}\mathbf{F}), \tag{49}$$

where $\mathbf{A}$ is an arbitrary second-order tensor and $\alpha\in\mathbb{R}$. Let $\{\mathbf{d}_i\}$ be the current basis. According to Gurtin et al. (2010), because $\mathbf{F}$ is a two-point tensor, we write

$$\mathbf{F}=F_{ij}(\mathbf{d}_i\otimes\mathbf{e}_j),\ \ \mathbf{F}^{-1}=F^{-1}_{ij}(\mathbf{e}_i\otimes\mathbf{d}_j),\ \ \mathbf{F}^{\mathsf{T}}=F_{ij}(\mathbf{e}_j\otimes\mathbf{d}_i),\ \text{and}\ \ \mathbf{F}^{-\mathsf{T}}=F^{-1}_{ij}(\mathbf{d}_j\otimes\mathbf{e}_i). \tag{50}$$

In addition, the basis of the fourth-order tensors, obtained from the derivative between second-order tensors, one of which is a two-point tensor, must be written properly. For example, $\partial(\ln\mathbf{U})/\partial\mathbf{F}$ is expressed as follows ($\mathbf{e}_s\otimes\mathbf{e}_t\otimes\mathbf{d}_m\otimes\mathbf{e}_n$). Thus, the term $\mathbf{F}^{-1}\mathbf{A}$ in Equation (49) was developed as follows:

$$\mathbf{F}^{-1}\mathbf{A}\overset{(\mathrm{I})}{=}\mathbf{I}:(\mathbf{F}^{-1}\mathbf{A})\overset{(\mathrm{II})}{=}\delta_{su}\delta_{tn}(\mathbf{e}_s\otimes\mathbf{e}_t\otimes\mathbf{e}_u\otimes\mathbf{e}_n):\left[F^{-1}_{um}(\mathbf{e}_u\otimes\mathbf{d}_m)A_{mn}(\mathbf{d}_m\otimes\mathbf{e}_n)\right]\overset{(\mathrm{III})}{=}$$

$$\overset{(\mathrm{III})}{=}\delta_{su}\delta_{tn}F^{-1}_{um}A_{mn}\left[(\mathbf{e}_s\otimes\mathbf{e}_t)\otimes(\mathbf{e}_u\otimes\mathbf{e}_n)\right]:\left[(\mathbf{e}_u\otimes\mathbf{d}_m)(\mathbf{d}_m\otimes\mathbf{e}_n)\right]\overset{(\mathrm{IV})}{=}\delta_{su}\delta_{tn}F^{-1}_{um}A_{mn}\left[(\mathbf{e}_u\otimes\mathbf{e}_n):(\mathbf{e}_u\otimes\mathbf{d}_m)(\mathbf{d}_m\otimes\mathbf{e}_n)\right](\mathbf{e}_s\otimes\mathbf{e}_t)\overset{(\mathrm{V})}{=}$$

$$\overset{(\mathrm{V})}{=}\delta_{su}\delta_{tn}F^{-1}_{um}A_{mn}\left[(\mathbf{d}_m\otimes\mathbf{e}_u)(\mathbf{e}_u\otimes\mathbf{e}_n):(\mathbf{d}_m\otimes\mathbf{e}_n)\right](\mathbf{e}_s\otimes\mathbf{e}_t)\overset{(\mathrm{VI})}{=}\delta_{tn}F^{-1}_{sm}A_{mn}\left[(\mathbf{d}_m\otimes\mathbf{e}_n):(\mathbf{d}_m\otimes\mathbf{e}_n)\right](\mathbf{e}_s\otimes\mathbf{e}_t)\overset{(\mathrm{VII})}{=}$$

$$\overset{(\mathrm{VII})}{=}\delta_{tn}F^{-1}_{sm}(\mathbf{e}_s\otimes\mathbf{e}_t\otimes\mathbf{d}_m\otimes\mathbf{e}_n):A_{mn}(\mathbf{d}_m\otimes\mathbf{e}_n)\Rightarrow\mathbf{F}^{-1}\mathbf{A}=\delta_{tn}F^{-1}_{sm}(\mathbf{e}_s\otimes\mathbf{e}_t\otimes\mathbf{d}_m\otimes\mathbf{e}_n):\mathbf{A}\,, \tag{51}$$

where in step (I) we used Equation $(47)_1$, in step (II) we applied Equations $(48)_1$ and $(50)_2$, in step (III) we applied Equation $(46)_1$, in step (IV) we applied Equation (45), in step (V) we applied Equation $(44)_1$, in step (VI) we applied Equation $(46)_2$,

and in step (VII) we applied Equations (45) and $(46)_1$. Subsequently, the term $\mathbf{F}^{-1}\mathbf{F}^{-\mathsf{T}}\mathbf{A}^{\mathsf{T}}\mathbf{F}$ in Equation (49) is developed as

$$\mathbf{F}^{-1}\mathbf{F}^{-\mathsf{T}}\mathbf{A}^{\mathsf{T}}\mathbf{F} = \left(\mathbf{F}^{\mathsf{T}}\mathbf{A}\mathbf{F}^{-1}\mathbf{F}^{-\mathsf{T}}\right)^{\mathsf{T}} \overset{(I)}{=} \bar{\mathbf{I}} : \left(\mathbf{F}^{\mathsf{T}}\mathbf{A}\mathbf{F}^{-1}\mathbf{F}^{-\mathsf{T}}\right) \overset{(II)}{=}$$

$$\overset{(II)}{=} \delta_{sv}\delta_{tu}\left(\mathbf{e}_s \otimes \mathbf{e}_t \otimes \mathbf{e}_u \otimes \mathbf{e}_v\right) : \left[F_{mu}\left(\mathbf{e}_u \otimes \mathbf{d}_m\right) A_{mn}\left(\mathbf{d}_m \otimes \mathbf{e}_n\right) F^{-1}_{nw}\left(\mathbf{e}_n \otimes \mathbf{d}_w\right) F^{-1}_{vw}\left(\mathbf{d}_w \otimes \mathbf{e}_v\right)\right] \overset{(III)}{=}$$

$$\overset{(III)}{=} \delta_{sv}\delta_{tu}F_{mu}A_{mn}F^{-1}_{nw}F^{-1}_{vw}\left[\left(\mathbf{e}_u \otimes \mathbf{e}_v\right) : \left(\mathbf{e}_u \otimes \mathbf{d}_m\right)\left(\mathbf{d}_m \otimes \mathbf{e}_n\right)\left(\mathbf{e}_n \otimes \mathbf{d}_w\right)\left(\mathbf{d}_w \otimes \mathbf{e}_v\right)\right]\left(\mathbf{e}_s \otimes \mathbf{e}_t\right) \overset{(IV)}{=}$$

$$\overset{(IV)}{=} \delta_{sv}\delta_{tu}F_{mu}A_{mn}F^{-1}_{nw}F^{-1}_{vw}\left[\left(\mathbf{d}_m \otimes \mathbf{e}_u\right)\left(\mathbf{e}_u \otimes \mathbf{e}_v\right)\left(\mathbf{e}_v \otimes \mathbf{d}_w\right)\left(\mathbf{d}_w \otimes \mathbf{e}_n\right) : \left(\mathbf{d}_m \otimes \mathbf{e}_n\right)\right]\left(\mathbf{e}_s \otimes \mathbf{e}_t\right) \overset{(V)}{=}$$

$$\overset{(V)}{=} F_{mt}A_{mn}F^{-1}_{nw}F^{-1}_{sw}\left[\left(\mathbf{d}_m \otimes \mathbf{e}_n\right) : \left(\mathbf{d}_m \otimes \mathbf{e}_n\right)\right]\left(\mathbf{e}_s \otimes \mathbf{e}_t\right) \overset{(VI)}{=} F_{mt}F^{-1}_{nw}F^{-1}_{sw}\left(\mathbf{e}_s \otimes \mathbf{e}_t \otimes \mathbf{d}_m \otimes \mathbf{e}_n\right) : A_{mn}\left(\mathbf{d}_m \otimes \mathbf{e}_n\right) \Rightarrow$$

$$\Rightarrow \mathbf{F}^{-1}\mathbf{F}^{-\mathsf{T}}\mathbf{A}^{\mathsf{T}}\mathbf{F} = F_{mt}F^{-1}_{nw}F^{-1}_{sw}\left(\mathbf{e}_s \otimes \mathbf{e}_t \otimes \mathbf{d}_m \otimes \mathbf{e}_n\right) : \mathbf{A}\,, \tag{52}$$

where in step (I) we used Equation $(47)_2$, in step (II) we used Equations $(48)_2$ and (50), in step (III) we used Equations $(46)_1$ and (45), in step (IV) we used Equation $(44)_2$, in step (V) we used Equation $(46)_2$, and in step (VI) we applied Equations (45) and $(46)_1$. Substituting Equations (51) and (52) into Equation (49) we obtain

$$D\mathbf{K}(\mathbf{F})[\mathbf{A}] = \frac{1}{2}\left(\delta_{tn}F^{-1}_{sm} + F_{mt}F^{-1}_{nw}F^{-1}_{sw}\right)\left(\mathbf{e}_s \otimes \mathbf{e}_t \otimes \mathbf{d}_m \otimes \mathbf{e}_n\right) : \mathbf{A}\,, \tag{53}$$

and as $D\mathbf{K}(\mathbf{F})[\mathbf{A}] = \partial(\ln \mathbf{U})/\partial\mathbf{F} : \mathbf{A}$, we obtain

$$\frac{\partial(\ln \mathbf{U})}{\partial \mathbf{F}} = \frac{1}{2}\left(\delta_{tn}F^{-1}_{sm} + F_{mt}F^{-1}_{nw}F^{-1}_{sw}\right)\left(\mathbf{e}_s \otimes \mathbf{e}_t \otimes \mathbf{d}_m \otimes \mathbf{e}_n\right) \Rightarrow \frac{\partial(\ln \mathbf{U})_{st}}{\partial F_{mn}} = \frac{1}{2}\left(\delta_{tn}F^{-1}_{sm} + F_{mt}F^{-1}_{nw}F^{-1}_{sw}\right). \tag{54}$$

Differentiating Equation (54) with respect to F_{op}, we obtain

$$\frac{\partial^2(\ln \mathbf{U})_{st}}{\partial F_{mn}\partial F_{op}} = \frac{1}{2}\left(-\delta_{tn}F^{-1}_{so}F^{-1}_{pm} + \delta_{mo}\delta_{tp}F^{-1}_{nx}F^{-1}_{sx} - F_{mt}F^{-1}_{no}F^{-1}_{px}F^{-1}_{sx} - F_{mt}F^{-1}_{nx}F^{-1}_{so}F^{-1}_{px}\right). \tag{55}$$

The strategy used in this appendix for writing strain tensor derivatives directly in the global direction is general and simple. This can be applied to obtain the derivatives of complex strain tensors, such as the tangent strain tensor (see Equation (8)),

$$\mathbf{G}(\mathbf{U}) = \frac{\varepsilon}{\pi}\cos^2\left[\pi\left(\frac{1}{\varepsilon} - \frac{1}{2}\right)\right]\left\{\tan\left(\pi\left(\frac{1}{\varepsilon}\mathbf{U} - \frac{1}{2}\mathbf{I}\right)\right) - \tan\left[\pi\left(\frac{1}{\varepsilon} - \frac{1}{2}\right)\right]\mathbf{I}\right\}. \qquad \varepsilon > 1.0 \tag{56}$$

ACKNOWLEDGMENTS

We thank Fundação de Amparo à Pesquisa do Estado de Minas Gerais (FAPEMIG), Conselho Nacional de Desenvolvimento Científico e Tecnológico (CNPq), and Coordenação de Aperfeiçoamento de Pessoal de Nível Superior (CAPES) for their research financial supports. Also, we thank the valuable contributions of the editor that improved the presentation of this work.

Author's Contribuitions: Conceptualization, M Greco and DB Vasconcellos; Methodology, M Greco and DB Vasconcellos; Investigation, DB Vasconcellos; Writing - original draft, DB Vasconcellos; Writing - review & editing, M Greco and DB Vasconcellos; Supervision, M Greco.

Editor: Rogério José Marczak

References

Arruda, E. M., Boyce, M. C. (1993). A three-dimensional constitutive model for the large stretch behavior of rubber elastic materials, Journal of the Mechanics and Physics of Solids 41: 389-412.

Boujelben, A., Ibrahimbegovic, A. (2017). Finite-strain three-dimensional solids with rotational degrees of freedom: non-linear statics and dynamics, Advanced Modeling and Simulation in Engineering Sciences 4: 1-24.

Cao, J., Ding, X.-F., Yin, Z.-N., Xiao, H. (2016). Large elastic deformations of soft solids up to failure: new hyperelastic models with error estimation, Acta Mechanica 228: 1165-1175.

Coda, H. B., Greco, M. (2004). A simple FEM formulation for large deflection 2D frame analysis based on position description, Computer Methods in Applied Mechanics and Engineering 193: 3541-3557.

Coda, H. B., Paccola, R. R. (2007). An alternative positional FEM formulation for geometrically non-linear analysis of shells: Curved triangular isoparametric elements, Computational Mechanics 40: 185-200.

Curnier, A., Rakotomanana, L. (1991). Generalized strain and stress measures: Critical survey and new results, Engineering Transactions 39: 461-538.

Curnier, A., Zysset, Ph. (2006). A family of metric strains and conjugate stresses, prolonging usual material laws from small to large deformation, International Journal of Solids and Structures 43: 3057-3086.

Dal, H., Açıkgöz, K., Badienia, Y. (2021). On the performance of isotropic hyperelastic constitutive models for rubber-like materials: A state of the art review, Applied Mechanics Reviews 73: 020802.

Darijani, H., Naghdabadi, R. (2013). Kinematics and kinetics modeling of thermoelastic continua based on the multiplicative decomposition of the deformation gradient, International Journal of Engineering Science 62: 56-69.

Darijani, H., Naghdabadi, R., Kargarnovin, M. H. (2010). Hyperelastic materials modelling using a strain measure consistent with the strain energy postulates, Proc. Inst. Mech. Eng., Part C, Journal of Mechanical Engineering Science 224: 591-602.

Doyle, T. C., Ericksen, J. L. (1956). Nonlinear elasticity, Advances in Applied Mathematics 4: 53-115.

Farahani, K., Naghdabadi, R. (2003). Basis free relations for the conjugate stresses of the strains based on the right stretch tensor, International Journal of Solids and Structures 40: 5887-5900.

Fitzgerald, J. E. (1980). A tensorial Hencky measure of strain and strain rate for finite deformations, Journal of Applied Physics 51: 5111-5115.

Fosdick, R. L., Serrin, J. (1979). On the impossibility of linear Cauchy and Piola-Kirchhoff constitutive theories for stress in solids, Journal of Elasticity 9: 83-89.

Greco, M., Coda, H. B. (2006). Positional FEM formulation for flexible multi-body dynamic analysis, Journal of Sound and Vibration 290: 1141-1171.

Greco, M., Peixoto, D. H. N. (2022). Comparative assessments of strain measures for nonlinear analysis of truss structures at large deformations, Engineering Computations 39: 1621-1641.

Gurtin, M. E., Fried, E., Anand, L. (2010). The Mechanics and thermodynamics of continua, Cambridge University Press (New York).

Hill, R. (1968). On constitutive inequalities for simple materials – I, Journal of the Mechanics and Physics of Solids 16: 229-242.

Hill, R. (1978). Aspects of invariance in solid mechanics, Advances in applied mechanics 18: 1-75.

Holzapfel, G. A. (2000). Nonlinear solids mechanics – A continuum approach for engineering, John Wiley & Sons (Chichester).

Horgan, C. O., Saccomandi G. (2006). Phenomenological hyperelastic strain-stiffening constitutive models for rubber, Rubber Chemistry and Technology 79: 152-169.

Itskov, M. (2004). On the application of the additive decomposition of generalized strain measures in large strain plasticity, Mechanics Research Communications 31: 507-517.

Itskov, M. (2019). Tensor algebra and tensor analysis for engineers, Springer (Cham).

Kang, J., Tan, L.-X., Liu, Q.P., Wang, S.Y., Bruhns, O. T., Xiao, H. (2024). Unified and accurate simulation for large elastic strain responses of rubberlike soft materials under multiple modes of loading, Continuum Mechanics and Thermodynamics 32: 155-169.

Korbeynikov, S. N. (2019). Objective symmetrically physical strain tensors, conjugate stress tensors and Hill's linear isotropic hyperelastic materials models, Journal of Elasticity 136: 159-187.

Korbeynikov, S. N. (2022). Hyperelasticity models extending Hooke's law from small to moderate strains and experimental verification of their scope of application, International Journal of Solids and Structures 252: 111815.

Korbeynikov, S. N. (2023). Families of Hooke-like isotropic hyperelastic material models and their rate formulations, Archive of Applied Mechanics 93: 3863-3893.

Korbeynikov, S. N., Larichkin, A. Y. (2023). Simulating body deformations with initial stresses using Hooke-like isotropic hypoelasticity models based on corotational stress rates, ZAMM - Journal of Applied Mathematics and Mechanics 104: e202300568.

Lateefi, M. M., Kumar, D., Sarangi, S. (2022). An alternative form of energy density demonstrating the severe strain-stiffening in thin spherical and cylindrical shells, Theorical and Applied Mechanical Letters 12: 100361.

Liang, X., Dong, J., Liu, J., Xu, P., Li, K. (2020). Indentation of a prestretched strain-stiffening elastomer, Mathematics and Mechanics of Solids 25: 2118-2131.

Mal, A. K., Singh, S. J. (1991). Deformation of elastic solids. Prentice-Hall (New Jersey).

Peixoto, D. H. N., Greco, M. (2022). Presentation of a new family of strain measures based on the hyperbolic tangent function, In MECSOL 2022, Campinas, Brasil.

Peixoto, D. H. N., Greco, M., Vasconcellos, D. B. (2024). A new family of strain tensors based on the hyperbolic sine function, Latin American Journal of Solids and Structures 21: e529.

Salamatova, V. Y., Vassilevski, Y. V., Wang, L. (2018). Finite element models of hyperelastic materials based on a new strain measure, Differential Equations 54: 971-978.

Saucedo-Mora, L., García-Bañales, O., Montáns, F. J., Benítez, J. M. (2021). A two-parameter strain energy function for brain matter: An extension of the Hencky model to incorporate locking, Brain Multiphysics 2: 100036.

Sautter, K. B., Meßmer, M., Teschemacher, T., Bletzinger, K.-U. (2022). Limitation of the St. Venant-Kirchhoff material model in large strain regimes, International Journal of Non-Linear Mechanics 147: 104207.

Santos, L. D., Maciel, D. N., Barros, R., Neto, J. A. D. N., Filho, J. N. D. S. (2024). Nonlinear analysis of plane frames considering hyperelastic models through the finite element positional method, Latin American Journal of Solids and Structures 21: e559.

Seth, B. R. (1964). Generalized strain measure with application to physical problems, Academic Press (Jerusalem).

Srinivasa, A. R. (2012). On the use of the upper triangular (or QR) decomposition for developing constitutive equations for Green-elastic materials, International Journal of Engineering Science 60: 1-12.

Treloar, L.R.G. (1975). The physics of rubber elasticity, Oxford University Press (Oxford).

Truesdell, C. A., Toupin, R. (1960). The classical field theories, Springer Verlag (Berlin).

Tsai, S. W., Melo, J. D. D. (2014). An invariant-based theory of composites, Composites Science and Technology 100: 237-243.

Volokh, K. Y. (2004). Comments and authors' reply on ''Linear stress-strain relations in nonlinear elasticity'' by A. Chiskis and R. Parnes, (Acta Mech. 146, 109–113, 2001), Acta Mechanica 171: 241-245.

Wheeler, L. T., Casey, J. (2011). Fréchet differentiation of the stretch and rotation tensors, Mathematics and Mechanics of Solids 16: 753-768.

Yuan, L., Gu, Z.-X., Yin, Z.-N., Xiao, H. (2015). New compressible hyper-elastic models for rubberlike materials, Acta Mechanica 226: 4059-4072.

Zenkert, D., Burman, M. (2009). Tension, compression and shear fatigue of a closed cell polymer foam, Composites Science and Technology 69: 785-792.